Highly enhanced oxidation of arsenite at the surface of birnessite in the presence of pyrophosphate and the underlying reaction mechanisms

Chaoyun Ying, Bruno Lanson, Cheng Wang, Xiaoming Wang, Hui Yin, Yupeng Yan, Wenfeng Tan, Fan Liu, Xionghan Feng

Highlights:

- As(III) oxidation by birnessite leads to Mn(II/III) species formation
- Manganite precipitation passivates birnessite surface and limits As(III) oxidation
- Presence of pyrophosphate in reactive medium enhances As(III) oxidation
- PP inhibits passivation forming soluble Mn(III) complexes
- Oxidation enhancement by chelates depends on the stability of Mn(III) complexes

Graphical Abstract

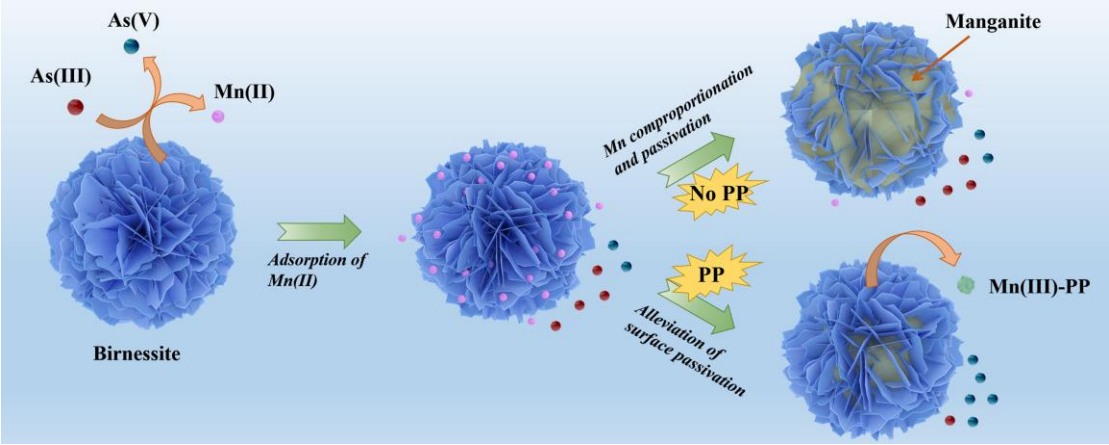

Highly enhanced oxidation of arsenite at the surface of birnessite in the presence of pyrophosphate and the underlying reaction mechanisms

Chaoyun Ying[a], *Bruno Lanson*[b], *Cheng Wang*[a], *Xiaoming Wang*[a], *Hui Yin*[a], *Yupeng Yan*[a], *Wenfeng Tan*[a], *Fan Liu*[a], *Xionghan Feng*[a,*]

[a]Key Laboratory of Arable Land Conservation (Middle and Lower Reaches of Yangtze River), Ministry of Agriculture, College of Resources and Environment, Huazhong Agricultural University, Wuhan 430070, China.

[b]Univ. Grenoble Alpes, CNRS, Univ. Savoie Mont Blanc, IRD, Univ. Gustave Eiffel, ISTerre, F-38000 Grenoble, France

*Corresponding author:
Xionghan Feng,
Tel: +86 27 87280271; Fax: +86 27 87288618; E-mail: fxh73@mail.hzau.edu.cn

Keywords: *birnessite; arsenite oxidation; pyrophosphate; Mn(III) chelating; depassivation*

ABSTRACT

Manganese(IV) oxides, and more especially birnessite, rank among the most efficient metal oxides for As(III) oxidation and subsequent sorption, and thus for arsenic immobilization. Efficiency is limited however by the precipitation of low valence Mn (hydr)oxides at the birnessite surface that leads to its passivation. The present work investigates experimentally the influence of chelating agents on this oxidative process. Specifically, the influence of sodium pyrophosphate (PP), an efficient Mn(III) chelating agent, on As(III) oxidation by birnessite was investigated using batch experiments and different arsenic concentrations at circum-neutral pH. In the absence of PP, Mn(II/III) species are continuously generated during As(III) oxidation and adsorbed to the mineral surface. Field emission-scanning electron microscopy, synchrotron-based X-ray diffraction and Fourier transform infrared spectroscopy indicate that manganite is formed, passivating birnessite surface and thus hampering the oxidative process. In the presence of PP, generated Mn(II/III) species form soluble complexes, thus inhibiting surface passivation and promoting As(III) conversion to As(V) from 60% in the absence of PP to 100% with 3 mM PP (0.5 mM initial As(III)). Enhancement of As(III) oxidation by Mn oxides strongly depends on the affinity of the chelating agent for Mn(III) and from the induced stability of Mn(III) complexes. Compared to PP, the positive influence of oxalate, for example, on the oxidative process is more limited. The present study thus provides new insights into the possible optimization of arsenic removal from water using Mn oxides, and on the possible environmental control of arsenic contamination by these

ubiquitous non-toxic mineral species.

1. Introduction

In natural waters, arsenite, As(III), mainly occurs as the neutral species H_3AsO_3, while arsenate, As(V), is present as $H_2AsO_4^-$ or $HAsO_4^{2-}$ oxyanions under a variety of pH conditions (Cerkez et al., 2015). Both forms are highly toxic and carcinogenic, and the maximum contaminant level for arsenic in drinking water defined by the World Health Organization (WHO) is thus extremely low at 10 µg/L. Arsenite is even more toxic and mobile than arsenate in aqueous environments (Cerkez et al., 2015; Fischel et al., 2015; Neppolian et al., 2010) and more difficult to remove owing to its low affinity for sorbents (Luong et al., 2018). Oxidizing As(III) into the more easily extractable As(V) thus appears appropriate to achieve efficient arsenic immobilization and removal (Zhang et al., 2016).

Although As(III) is stable in homogeneous systems (Katsoyiannis and Zouboulis, 2004; Tsang et al., 2007), a variety of metal oxides such as iron (hydr)oxides (Amirbahman et al., 2006; Wang and Giammar, 2015; Yang et al., 2017; Zhao et al., 2011) and titanium oxides (Dutta et al., 2004; Ferguson et al., 2005; Guan et al., 2012) can induce its oxidation directly or indirectly. As a consequence, As concentration in natural aqueous environments is essentially controlled by interactions with mineral surfaces. Composite oxides have also been developed to enhance their efficiency as oxidants and adsorbents for both As(III) and As(V) (Chakravarty et al., 2002; Feng et al., 2006a; Ma et al., 2020; McCann et al., 2018; Wu et al., 2018; Ying et al., 2012;

Zhang et al., 2007; Zhang et al., 2018; Zheng et al., 2020). Manganese (Mn) oxides can also oxidize As(III) (Manning et al., 2002; Scott and Morgan, 1995), as reported in natural lacustrine environments (Oscarson et al., 1980, 1981a, 1981b), and Mn oxides have a key role in As geochemical cycling (Driehaus et al., 1995; Nesbitt et al., 1998; Scott and Morgan, 1995; Tournassat et al., 2002). Produced Mn(II) adsorbs to the particle edges, thus potentially blocking reactive sites for further oxidation (Villalobos et al., 2014). Lafferty and coworkers (Lafferty et al., 2010a, 2010b, 2011) identified Mn(II) as the unique reduced product during the initial phase of the reaction. They also concluded that Mn(III) was subsequently formed as the result of the comproportionation of Mn(II) adsorbed onto birnessite surface rather than from Mn(IV) reduction, as previously hypothesized (Nesbitt et al., 1998). Manganite (γ-Mn(III)OOH) then accumulates at the birnessite surface leading to its passivation, as Mn(III) sites are less reactive than Mn(IV) ones with respect to As(III) oxidation, as shown by DFT calculations (Zhu et al., 2009). Finally, Lafferty and coworkers showed that As(V) was the sole As species adsorbed to manganese oxides (Lafferty et al., 2010a, 2010b, 2011).

In contrast to the optimization of the oxidizing solid, little attention has been paid to the influence of additional chemicals present in the reactive medium. For example, the presence of phosphate in solution hampers As(III) oxidation by Mn oxides (Chiu and Hering, 2000; Parikh et al., 2010), whereas that of tartaric acid promotes it (Feng et al., 2006b). More generally, the presence in the reactive medium of compounds chelating Mn, and more especially Mn(III), is expected to enhance the oxidative

process (Ma et al., 2020). With this respect, pyrophosphate (PP) appears especially relevant owing to its strong affinity for Mn(III) (Liu et al., 2019; Marafatto et al., 2018; Parker et al., 2004; Soldatova et al., 2017). The relevance of PP is further increased by its common formation in natural environments, as the simplest polymer of orthophosphate resulting from the breakdown of ATP and ADP (Klewicki and Morgan, 1999b; Trouwborst et al., 2006).

The present experimental work thus investigated in detail the influence of PP on As(III) oxidation by the Mn oxide birnessite at circumneutral pH. The effect of PP addition on the completeness of the reaction and the involved reaction mechanisms were specifically studied from a combination of wet chemical analyses and of solid phase characterization using electron microscopy, X-ray diffraction, X-ray absorption and photoelectron spectroscopies, and infrared spectroscopy.

2. Materials and Methods

2.1 Chemicals

All chemical used in the present study were purchased from Sinopharm Chemical Reagent, except for the manganese(III) acetate dihydrate which was purchased from Sigma Chemical. All chemicals were of analytical grade. Atomic absorption spectroscopy Mn standard was prepared by dilution of a 1000 mg/L standard. Deionized water was used throughout the experiments.

2.2 Synthetic Acid Birnessite Preparation

Synthetic acid birnessite was prepared according to a method modified from that of McKenzie (1971). In brief, 45 mL of a 6 M HCl solution were added dropwise to 300 mL of a boiling 0.667 M solution of $KMnO_4$. The obtained suspension was stored at 60 °C for 12 h to increase birnessite crystallinity. Resulting solid was then washed with deionized water and centrifuged (10×) to remove K^+ and Cl^- in excess.

2.3 Batch As(III) Oxidation by Birnessite and Wet Chemical Analyses

Batch experiments were conducted using 50 mL of a 0.2 g/L suspension of the obtained synthetic birnessite at two As(III) concentrations (0.5 and 1 mM) in the presence/absence of sodium pyrophosphate (PP). When present, PP concentrations were 1, 2, 3, 4, 5, 8, and 10 mM, with a 2.5 mM NaCl background electrolyte. Mixed suspensions, whose pH was pre-adjusted to 7.2 using 0.2-1 mM HCl, were then stirred for 24 h. The solids were subsequently filtered and washed thoroughly with deionized water to remove residual dissolved ions.

In the absence of PP, As(V) was determined using the ammonium molybdenum method (Oscarson et al., 1980). In the presence of PP, As(III) and As(V) were determined using coupled LC-ICP-MS, As(III) and As(V) being separated by liquid chromatography (LC – Dionex IonPac AS19 Columns) using a four-component mobile phase (pH 10.22) at 1 mL/min flow rate. The outflow from the LC was directly connected to the inductively coupled plasma mass spectrometer (ICP-MS) for

As quantification. In specific experiments, PP was replaced by other chelating agents, such as sodium oxalate. In this case, As(V) and total As concentrations were measured using the molybdenum blue method (Feng et al., 2018), the concentration of As(III) being calculated from that of total As by subtracting As(V).

Mn concentration in solution was determined using atomic absorption spectrometry (AAS – Agilent Technologies 200 series). In addition, concentration of Mn(III)-PP complexes were determined with a UV-Vis spectrophotometer (Agilent Technologies Cary 8454), using 10 mm path length cuvettes and the absorption peaks at 258 nm and 480 nm (Webb et al., 2005).

2.4 Characterization of the Solid Products.

2.4.1 Mn K-edge XANES and Mn speciation analysis

X-ray absorption near edge structure (XANES) spectroscopy data were collected at room temperature on the 1W1B beamline at the Beijing Synchrotron Radiation Facility (BSRF) over the 6.4–7.0 keV range (Mn K-edge). Energy calibration was systematically performed using a Mn metal foil before data collection. Mn K-edge spectra were averaged and background-subtracted using the following parameters: E_0 = 6538 eV, Rbkg = 1 Å and k-weight = 2.

2.4.2 Field emission scanning electron microscopy

Gold-coated samples were observed using a field-emission scanning electron microscope (FESEM – SU8010, Hitachi) with a maximum resolution of 1 nm. For high-resolution images, the microscope was operated at 10 kV using a working distance of 10-15 mm, and an in-lens secondary electron detector.

2.4.3 Synchrotron radiation X-ray powder diffraction

Synchrotron radiation X-ray powder diffraction (SR-XRD) was performed on the BL14B1 beamline of the Shanghai Synchrotron Radiation Facility (SSRF). Data were collected over the 2-45 ° 2θ range ($\lambda = 0.6895$ Å), with 30 s exposure times (Yang et al., 2015).

2.4.4 Fourier transform infrared (FTIR) spectroscopy

FTIR spectra were collected using a Bruker Vertex 70 spectrometer equipped with a deuterated triglycine sulfate detector (Bruker Optics Inc., Ettlingen, Germany). Spectra were measured over the 4000–400 cm^{-1} range with a 4 cm^{-1} resolution in transmission mode. Thirty-two scans were collected and averaged for each sample, the data being collected, processed, and analyzed with the OPUS program.

2.4.5 X-ray photoelectron spectroscopy

X-ray photoelectron spectra (XPS) were collected using a VG Multilab2000 X-ray photoelectron spectrometer with an Al K X-ray source (1486 eV) and a base pressure of 3×10^{-9} Torr in the analytical chamber. The scans were recorded using the large area mode. The survey scans were collected using a fixed pass energy of 100 eV and an energy step size of 1.0 eV, whereas the narrow scans have a pass energy of 25 eV and an energy step size of 0.1 eV. Spectra were charge-corrected to C*1s* with a binding energy of 284.80 eV collected from the surface adventitious carbon (Wang et al., 2010) and analyzed with the Avantage software. The parameters proposed by Ilton et al. (2016) and Bang et al. (2005) for the spectral fitting of Mn*3p* and As*3d* multiple peaks were used.

3. Results and Discussion

3.1 The Oxidation of As(III) by Birnessite with/without Chelating Agents

Based on their relative redox potentials, As(III) could be oxidized by dissolved oxygen under circum-neutral conditions ($\triangle$E for O_2/H_2O and As(V)/As(III) couples is 0.70 V at neutral pH). However, As(III) is mostly hydrophilic and present as neutral species below pH 9**,** and the kinetics of its oxidation by O_2 is very slow at neutral pH (Lan et al., 2018). Consistently, the control experiments performed in the absence of manganese oxides showed that As(III) was essentially stable over a 24 h period (Fig. S1).

In the absence of PP and under similar circum-neutral conditions, birnessite was able to oxidize ~ 35 % of the As(III) initially present (1 mM) to As(V) after 24 h (Fig. 1a), whereas ~10 % of As adsorbed/precipitated at the birnessite surface. The As(III) concentration dropped exponentially with time over the first 2 h. The application of a pseudo-first order model yielded an apparent As(III) oxidation rate constant (k) of 0.1804 ± 0.0349 h^{-1} (k_1) over this 2 h interval (Fig. 1b). The reaction slowed down over the subsequent 10 h with an apparent rate constant decreased by about one order of magnitude (k_2 = 0.0187 ± 0.0015 h^{-1}), most likely as the result of the formation of a Mn precipitate passivating birnessite surface (Lafferty et al., 2010a). After 12 h, As(III) was not oxidized by birnessite anymore, consistent with the following equations proposed for As(III) oxidation (Lafferty et al., 2010a, 2010b):

$$>Mn(IV)\text{-}OH + H_3As(III)O_3 + H^+ \rightarrow Mn(II) + H_2As(V)O_4^- + H_2O \quad (1)$$

$$>Mn(IV)\text{-}OH + Mn(II) + H_2O + H^+ \rightarrow 2\,(>Mn(III)\text{-}OH_2) \quad (2)$$

According to these equations, As(III) oxidation occurs as a two-electron transfer process, the formation of Mn(III) resulting from the comproportionation of surface-adsorbed Mn(II) and structural Mn(IV) (Eq. 2). The proportion of As(III) oxidized by birnessite over 24 h was doubled in the presence of 5 mM PP in solution compared to the PP-free system (Fig. 1a). In the presence of PP, As(III) oxidation was not significantly promoted over the first 2 hours, the apparent rate constant being 0.1993 ± 0.0125 h^{-1} (k_3, compared to k_1 = 0.1804 ± 0.0349 h^{-1} – Fig. 1b). Over the next

10 hours, As(III) oxidation was highly enhanced in the presence of 5 mM PP, however, with an apparent rate constant of 0.0438 ± 0.0101 h^{-1} (k_4). Moreover, addition of PP allowed releasing to solution As species initially adsorbed/precipitated at the birnessite surface (Fig. 1a). Enhancement of As(III) oxidation results from the chelation by PP of Mn(III) formed as the result of Eq. 2 and from the release of these complexes to solution (Eq. 3 – Klewicki and Morgan, 1999b):

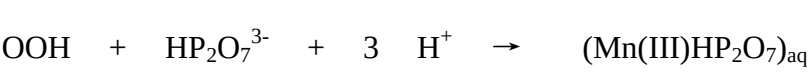

$$Mn(III)OOH + HP_2O_7^{3-} + 3\ H^+ \rightarrow (Mn(III)HP_2O_7)_{aq} + 2\ H_2O \quad (3)$$

Previous works showed that the excess of PP relative to Mn(III) should be at least fourfold to prevent the complexes from disproportionating (Qian et al., 2019). Thus, the difference between k_4 and the oxidation rate determined over the subsequent 12 hours (k_5 = 0.0091 ± 0.0025 h^{-1}) is likely related to the formation of Mn(III) that could not be fully chelated by PP (Fig. 1b).

Mn concentration in solution increased steadily in the presence of PP (Fig. 2a), nevertheless, as shown by the increase in intensity of the 258 nm UV-Vis absorption band (Fig. 2b) that is characteristic of the Mn(III)-PP complex (Soldatova et al., 2017). Consistently, the filtered solution appeared brownish red (Fig. S2), a color typical for Mn(III)-PP (Qian et al., 2019). High-valent Mn in solution, which hereafter refers to Mn(III)-PP, was quantified using Leucoberbelin Blue I (Zhu et al., 2017). The similar increases of aqueous Mn and of Mn(III)-PP indicated that Mn in solution was

233 overwhelmingly trivalent and present as Mn(III)-PP (Fig. 2a), consistent with XANES
234 results (Fig. S3). In the presence of both As(III) and As(V), Mn(III)-PP complexes
235 remained essentially stable over a 24 h interval in circum-neutral conditions (Table S1
236 and Fig. S4), consistent with the slow disproportionation reported for Mn(III)-PP at
237 circum-neutral pH (Qian et al., 2019). The minor decrease of Mn(III)-PP after 12 h is
238 possibly related to Mn oxides catalyzing PP hydrolysis (Wan et al., 2019).

239 The premise from Eq. 3 was supported by the experimental ratio between As(V),
240 produced from Eq. 1, aqueous Mn(III), produced from Eq. 2 and complexed by PP,
241 that steadily approached a 1:2 ratio with increasing PP in the presence of 0.5 mM
242 As(III) (Fig. S5), consistent with the stoichiometric ratio from Eqs. 1, 2. At low PP
243 concentration, the experimental ratio was significantly larger than 1:2 due to the
244 limited formation of Mn(III)-PP complexes. Increasing PP concentrations increased
245 Mn(III)-PP concentration in solution, birnessite being essentially dissolved over 24 h
246 in the presence of 10 mM PP and 1 mM As(III) (Fig. 3). The stoichiometric 1:2 ratio
247 between As(V) and Mn indicates that the oxidation of 1 mM As(III) required the
248 consumption of 2 mM Mn(IV), which exceeded the total Mn content in the
249 suspension. As a result, As(V) in solution never reached 1 mM even in the presence of
250 10 mM PP.

251 In addition, time-resolved As K-edge XANES spectroscopy was used to
252 determine the overall relative proportions of As(III) and As(V) in the reaction system
253 (Fig. S6). The position of As K absorption edge steadily shifted to higher energies
254 with increasing reaction time, showing the formation of As(V) at the expense of

As(III). Linear combination fitting (LCF) of the spectra unraveled the in-situ evolution kinetics of As(III) and As(V) species. The kinetic of As(III) oxidation using pseudo-first order model was linear over the first 180 min in the presence of PP (apparent rate constant k = 0.0049 ± 0.0001 h^{-1} – Fig. S7) and of the induced alleviation of surface passivation.

3.2 Identification of the Solid Products

Birnessite synthesized in the present study exhibited a uniform nano-flower morphology resulting from the assemblage of nano-flakes as revealed by FESEM (Fig. 4). When reacted with As(III) in the absence of PP, these nano-flowers appeared "filled" after 24 h of reaction, nano-flake edges becoming blurred, owing to the presence of precipitates at the particle surface. Increasing PP concentration in solution appeared to prevent the presence of these precipitates, leaving clean birnessite surfaces and thus significantly alleviating the passivation of birnessite surface.

SR-XRD patterns of the unreacted birnessite exhibited reflections at 0.723 (not shown), 0.361, 0.244, and 0.142 nm typical for birnessite (Fig. 5a). After reacting with 1 mM As(III) for 24 h in the absence of PP, additional reflections typical for manganite (ICDD#41-1379) were visible (Fig. 5a). Manganite precipitation was consistent with previous reports of birnessite interactions with aqueous Mn(II) at circum-neutral pH (Elzinga, 2011; Lefkowitz et al., 2013; Tournassat et al., 2002). Manganite peaks were not visible when PP was present in the reacting suspension,

however (Fig. 5a). None of the various manganese arsenate compounds with contrasting As: Mn molar ratios reported in the literature as secondary products of As(III) oxidation by birnessite (Moore et al., 1990; Tournassat et al., 2002) were detected either in the present study; pyrochroite ($Mn(OH)_2$ – ICDD#01-73-1133) was not observed either.

The 920 cm^{-1} band in the FT-IR spectrum of unreacted birnessite corresponded to the bending vibration of -OH located at vacancy sites (Fig. 5b – Yin et al., 2017; Zhao et al., 2012). After reaction with As(III) for 24 h in the absence of PP, new bands were visible at 1150, 1116, and 1087 cm^{-1} that were related to in-plane and out-of-plane bending modes of structural OH in manganite (Kohler et al., 1997; Lefkowitz et al., 2013), consistent with the presence of this phase shown by XRD data. Consistent with XRD data, these bands, typical for manganite, were not visible when PP was added to the reactive system.

In addition, XPS allowed identifying the chemical state of elements in the few uppermost atomic layers of solids and monitoring the evolution of Mn oxidation state at the birnessite surface. Mn*3p* XPS spectra were fitted using scale factors for the three multiplets used (Table S2) (Ilton et al., 2016), and the relative contributions of the different Mn oxidation states were quantified from the overall multiplet area (Fig. 6) (Table 1). The best fit to Mn*3p* spectrum of unreacted birnessite yielded 67% Mn(IV), 29% Mn(III), and 4% Mn(II), and the relative proportion of Mn(IV) at birnessite surface decreasing to 41% after reaction with As(III) in the absence of PP. Simultaneously, Mn(III) and Mn(II) increased to 50% and 9%, respectively, as the

298 result of As(III) oxidation. The significant increase of Mn(III) was consistent with the
299 key role played by Mn(IV) in the oxidation of As(III) and with the observed formation
300 of manganite at the particle surface (Figs. 4, 5). If PP was added to the reactive system,
301 the relative content of Mn(III) at the birnessite particle surface decreased (Table 1),
302 consistent with increased proportion of Mn(III)-PP in solution and the absence of
303 manganite formation. Enhancement of As(III) oxidation thus appeared to be induced by
304 the absence of birnessite surface passivation, resulting from manganite precipitation,
305 which was caused by Mn(III) complexation by PP. This enhancement was consistent
306 with theoretical calculations showing the higher affinity of both As(III) and As(V) for
307 Mn(IV) sites compared to Mn(III) sites and with the increased electron transfer rate
308 between As(III) and Mn(IV), compared to Mn(III) (Zhu et al., 2009). Finally, XPS
309 As*3d* spectra were characteristic of coexisting As(V) and As(III) species (Fig. S8),
310 whose binding energies were 45.5 ± 0.1 eV and 44.2 ± 0.1 eV, respectively (Table S3
311 – Bang et al., 2005). In the absence of PP, adsorbed/precipitated As was essentially
312 present as As(V), consistent with previous reports (Fig. S8 – Lafferty et al., 2010b).
313

314 ***3.3 The Effects of Different Chelating Agents on As(III) Oxidation***

315 Naturally occurring organic ligands other than PP, such as oxalate and citrate, are
316 also known to chelate Mn (Duckworth and Sposito, 2005; Jiang et al., 2019; Klewicki
317 and Morgan, 1999a; Mu et al., 2018; Taube, 1947; Zhang et al., 2019). As for PP, the
318 presence of oxalate in the reactive system promoted As(III) oxidation (by ~15% after

24 hours – Fig. 7a). Fig. 7b showed that little soluble Mn(III) was detected by leucoberbelin blue dye (Zhu et al., 2017), however. The limited enhancement of As(III) oxidation by oxalate was most likely linked to the reduced release of Mn(III) in solution, and thus to the lower ability of oxalate, compared to PP, to prevent surface passivation by chelating Mn(III) formed during the reaction (Eqs. 1, 2; Fig. 7b). The lower chelating activity of oxalate, compared to PP, was consistent with the respective stability constants of these complexing agents with Mn(III) (Log *K* are 9.98 and 11.7 for oxalate and PP, respectively) (Nico and Zasoski, 2001). Consistently, the first-order rate constant determined for the breakdown of Mn(III)-oxalate complexes ($Mn(III)(C_2O_4)^+$, $k = 1.97 \times 10^{-1}$ s^{-1}) was six orders of magnitude higher than that of Mn(III)-PP ($Mn(III)HP_2O_5$, $k = 3 \times 10^{-7}$ s^{-1}) under neutral conditions (Nicholson and Eley, 1997; Taube, 1947; Zhang et al., 2019). Moreover, organic ligands, such as oxalate, are considered as reducing agents interacting with Mn (hydr)oxides (Flynn and Catalano, 2019; Wang et al., 2018; Wang and Stone, 2006). Therefore, the ligands with both low reducing ability (or no redox activity) and high complexation ability with Mn(III), such as PP (Klewicki and Morgan, 1998), appear as ideal inhibitors of Mn(III) (hydr)oxide formation during reaction with As(III).

3.*4 Environmental significance*

Birnessite is ubiquitous in aquatic and terrestrial environments (Butterfield et al., 2013), where As(III) potentially coexists with pyrophosphate (PP). The major source

of PP in the environment appears to be ATP released from cells that can be hydrolyzed quickly to produce PP (Orriss et al., 2016). The above results provide a mechanistic understanding for the enhancement of As(III) oxidation by birnessite in the presence of PP through alleviation of surface passivation when the three species coexist.

As As(III) oxidation to As(V) is an effective pathway for arsenic detoxification in arsenic-containing drinking and waste water, birnessite is a potentially attractive oxidant to be used in large-scale treatment. Previous studies have shown that the presence of aqueous Fe(II) and Mn(II) may inhibit As(III) oxidation by birnessite (Gude et al., 2017), however, as these species are oxidized at the birnessite surface leading to its passivation and favoring As(III) (Ehlert et al., 2014). In the presence of PP, precipitation of Mn(III) on the surface of birnessite will likely be removed, thus alleviating surface passivation and enhancing As(III) oxidation. Hydrous ferric oxides, such as ferrihydrite (Ehlert et al., 2014), formed at the birnessite surface are also likely to be dissolved in the presence of PP (Kassim et al., 1984), thus releasing adsorbed As(III) to solution and promoting its oxidative interaction with birnessite.

4. Conclusions

As previously reported, oxidation of As(III) in presence of birnessite and at circum-neutral pH conditions proceeds as a two-electron transfer. The subsequent formation of Mn(III) results from the comproportionation of Mn(II) and Mn(IV) and leads to the precipitation of manganite at the surface of the initial birnessite particles.

Manganite precipitation passivates birnessite surface and restrains As(III) oxidation completeness. In the presence of PP, As(III) oxidation is significantly enhanced at circum-neutral pH. The major influence of PP on As(III) oxidation results from its strong chelating affinity for Mn(III), causing the relative content of Mn(III) at the birnessite surface to decrease. PP chelates newly formed Mn(III) and thus inhibits the formation of solid Mn(III) phases, such as manganite, that may passivate birnessite surface. The addition of PP to the oxidative system has major implications both for the efficiency of As(III) removal during water treatment and for the durability of birnessite as oxidizing catalyzer. Compared to other Mn(III) chelating agents, such as oxalate, pyrophosphate appears especially efficient in impeding surface passivation and limiting possible reductive activity.

Declaration of interest statement

Declarations of interest: none.

Acknowledgments

This work was supported by National Key R&D Program of China (No. 2017YFD0200201), and the National Natural Science Foundation of China (NSFC Grant Nos. 41471194).

Appendix. Supporting Information

Supplementary Information includes Tables S1-S3, Figs. S1-S8.

References

Amirbahman, A., Kent, D.B., Curtis, G.P. and Davis, J.A. 2006. Kinetics of sorption and abiotic oxidation of arsenic(III) by aquifer materials. Geochim. Cosmochim. Acta 70, 533–547.

Bang, S., Johnson, M.D., Korfiatis, G.P. and Meng, X. 2005. Chemical reactions between arsenic and zero-valent iron in water. Water Res. 39(5), 763-770.

Butterfield, C.N., Soldatova, A.V., Lee, S.W., Spiro, T.G. and Tebo, B.M. 2013. Mn(II,III) oxidation and MnO_2 mineralization by an expressed bacterial multicopper oxidase. Proc. Natl. Acad. Sci. U. S. A. 110(29), 11731-11735.

Cerkez, E.B., Bhandari, N., Reeder, R.J. and Strongin, D.R. 2015. Coupled redox transformation of chromate and arsenite on ferrihydrite. Environ. Sci. Technol. 49(5), 2858-2866.

Chakravarty, S., Dureja, V., Bhattacharyya, G., Maity, S. and Bhattacharjee, S. 2002. Removal of arsenic from groundwater using low cost ferruginous manganese ore. Water Res. 36, 625–632.

Chiu, V.Q. and Hering, J.G. 2000. Arsenic adsorption and oxidation at manganite surfaces. 1. Method for simultaneous determination of adsorbed and dissolved arsenic species. Environ. Sci. Technol. 34, 2029-2034.

Driehaus, W., Seith, R. and Jekel, M. 1995. Oxidation of arsenate(III) with manganese oxides in water treatment. Water Res. 29, 297-305.

Duckworth, O.W. and Sposito, G. 2005. Siderophore-manganese(III) interactions. I. Air-oxidation of manganese(ll) promoted by desferrioxamine B. Environ. Sci. Technol. 39(16), 6037-6044.

Dutta, P.K., Ray, A.K., Sharma, V.K. and Millero, F.J. 2004. Adsorption of arsenate and arsenite on titanium dioxide suspensions. J. Colloid Interface Sci. 278(2), 270-275.

Ehlert, K., Mikutta, C. and Kretzschmar, R. 2014. Impact of birnessite on arsenic and iron speciation during microbial reduction of arsenic-bearing ferrihydrite. Environ. Sci. Technol 48(19), 11320-11329.

Elzinga, E.J. 2011. Reductive transformation of birnessite by aqueous Mn(II). Environ. Sci. Technol. 45(15), 6366-6372.

Feng, X., Tan, W., Liu, F., Ruan, H.D. and He, J. 2006a. Oxidation of As^{III} by several manganese oxide minerals in absence and presence of goethite. Acta Geol. Sin. 80(2), 249-256.

Feng, X., Wang, P., Shi, Z., Kwon, K.D., Zhao, H., Yin, H., Lin, Z., Zhu, M., Liang, X., Liu, F. and Sparks, D.L. 2018. A quantitative model for the coupled kinetics of arsenic adsorption/desorption and oxidation on manganese oxides. Environ. Sci. Technol Letter 5, 175−180.

Feng, X., Zu, Y., Tan, W. and Liu, F. 2006b. Arsenite oxidation by three types of manganese oxides. J. Environ. Sci. 18(2), 292-298.

Ferguson, M.A., Hoffmann, M.R. and Hering, J.G. 2005. TiO2-photocatalyzed As (III) oxidation in

aqueous suspensions: reaction kinetics and effects of adsorption. Environ. Sci. Technol. 39(6), 1880-1886.

Fischel, M.H.H., Fischel, J.S., Lafferty, B.J. and Sparks, D.L. 2015. The influence of environmental conditions on kinetics of arsenite oxidation by manganese-oxides. Geochem. Trans. 16(15).

Flynn, E.D. and Catalano, J.G. 2019. Reductive transformations of layered manganese oxides by small organic acids and the fate of trace metals. Geochim. Cosmochim. Acta 250, 149-172.

Guan, X., Du, J., Meng, X., Sun, Y., Sun, B. and Hu, Q. 2012. Application of titanium dioxide in arsenic removal from water: a review. J. Hazard. Mater. 215, 1-16.

Gude, J.C.J., Rietveld, L.C. and van Halem, D. 2017. As(III) oxidation by MnO_2 during groundwater treatment. Water Res. 111, 41-51.

Harrington, J.M., Parker, D.L., Bargar, J.R., Jarzecki, A.A., Tebo, B.M., Sposito, G. and Duckworth, O.W. 2012. Structural dependence of Mn complexation by siderophores: Donor group dependence on complex stability and reactivity. Geochimica et Cosmochimica Acta 88, 106-119.

Ilton, E.S., Post, J.E., Heaney, P.J., Ling, F.T. and Kerisit, S.N. 2016. XPS determination of Mn oxidation states in Mn (hydr)oxides. Appl. Surf. Sci. 366, 475-485.

Jiang, B., Gong, Y., Gao, J., Sun, T., Liu, Y., Oturan, N. and Oturan, M.A. 2019. The reduction of Cr(VI) to Cr(III) mediated by environmentally relevant carboxylic acids: State-of-the-art and perspectives. J. Hazard. Mater. 365, 205-226.

Kassim, J., Gafoor, S. and Adams, W. 1984. Ferrihydrite in pyrophosphate extracts of podzol B horizons. Clay Miner. 19(1), 99-106.

Katsoyiannis, I.A. and Zouboulis, A.I. 2004. Application of biological processes for the removal of arsenic from groundwaters. Water Res. 38(1), 17-26.

Klewicki, J.K. and Morgan, J.J. 1998. Kinetic Behavior of Mn(III) Complexes of Pyrophosphate, EDTA, and Citrate. Environ. Sci. Technol 32, 2916-2922.

Klewicki, J.K. and Morgan, J.J. 1999a. Dissolution of β-MnOOH particles by ligands Pyrophosphate, ethylenediaminetetraacetate, and citrate. Geochim. Cosmochim. Acta 63, 3017–3024.

Klewicki, J.K. and Morgan, J.J. 1999b. Dissolution of β-MnOOH particles by ligands: Pyrophosphate, ethylenediaminetetraacetate, and citrate. Geochim. Cosmochim. Acta 63(19/20), 3017-3024.

Kohler, T., Armbruster, T. and Libowitzky, E. 1997. Hydrogen bonding and Jahn-Teller distortion in groutite, α-MnOOH, and manganite, γMnOOH, and their relations to the manganese dioxides ramsdellite and pyrolusite. J. Solid State Chem. 133, 486-500.

Lafferty, B.J., Ginder-Vogel, M. and Sparks, D.L. 2011. Arsenite oxidation by a poorly-crystalline manganese oxide. 3. Arsenic and manganese desorption. Environ. Sci. Technol. 45(21), 9218-9223.

Lafferty, B.J., Ginder-Voger, M. and Sparks, D.L. 2010a. Arsenite oxidation by a poorly crystalline manganese-oxide 1. Stirred-flow experiments. Environ. Sci. Technol. 44(22), 8460-8466.

Lafferty, B.J., Ginder-Voger, M., Zhu, M., Livi, K.J.T. and Sparks, D.L. 2010b. Arsenite oxidation by a poorly crystalline manganese-oxide. 2. Results from X-ray absorption spectroscopy and X-ray diffraction. Environ. Sci. Technol. 44(22), 8467-8472.

Lan, S., Ying, H., Wang, X., Liu, F., Tan, W., Huang, Q., Zhang, J. and Feng, X. 2018. Efficient catalytic As(III) oxidation on the surface of ferrihydrite in the presence of aqueous Mn(II). Water Res. 128, 92-101.

Lefkowitz, J.P., Rouff, A.A. and Elzinga, E.J. 2013. Influence of pH on the reductive transformation of

463 birnessite by aqueous Mn(II). Environ. Sci. Technol. 47(18), 10364-10371.
464 Liu, W., Sun, B., Qiao, J. and Guan, X. 2019. Influence of pyrophosphate on the generation of soluble
465 Mn(III) from reactions involving Mn oxides and Mn(VII). Environ. Sci. Technol. 53(17),
466 10227-10235.
467 Luong, V.T., Kurz, E.E.C., Hellriegel, U., Luu, T.L., Hoinkis, J. and Bundschuh, J. 2018. Iron-based
468 subsurface arsenic removal technologies by aeration: a review of the current state and future
469 prospects. Water Res. 133, 110-122.
470 Luther, G.W., Ruppel, D.T. and Burkhard, C. (1998), ACS Publications.
471 Ma, L., Cai, D. and Tu, S. 2020. Arsenite simultaneous sorption and oxidation by natural ferruginous
472 manganese ores with various ratios of Mn/Fe. Chem. Eng. J. 382, 123040.
473 Manning, B.A., Fendorf, S.E., Bostick, B. and Suarez, D.L. 2002. Arsenic (III) oxidation and arsenic (V)
474 adsorption reactions on synthetic birnessite. Environ. Sci. Technol. 36(5), 976-981.
475 Marafatto, F.F., Lanson, B. and Peña, J. 2018. Crystal growth and aggregation in suspensions of δ-MnO2
476 nanoparticles: implications for surface reactivity. Environ. Sci. Nano 5(2), 497-508.
477 McCann, C.M., Peacock, C.L., Hudson-Edwards, K.A., Shrimpton, T., Gray, N.D. and Johnson, K.L.
478 2018. In situ arsenic oxidation and sorption by a Fe-Mn binary oxide waste in soil. J. Hazard.
479 Mater. 342, 724-731.
480 McKenzie, R.M. 1971. The synthesis of birnessite, cryptomelane, and some other oxides and hydroxides
481 of manganese. Miner. Mag. 38, 493-502.
482 Moore, J.N., Walker, J.R. and Hayes, T.H. 1990. Reaction scheme for the oxidation of As(III) to As(V)
483 by birnessite. Clay. Clay Miner. 38(5), 549-555.
484 Mu, Y., Jiang, X., Ai, Z., Jia, F. and Zhang, L. 2018. Mn^{2+} promoted Cr(VI) reduction with oxalic acid:
485 The indispensable role of In-situ generated Mn^{3+}. J. Hazard. Mater. 343, 356-363.
486 Neppolian, B., Doronila, A. and Ashokkumar, M. 2010. Sonochemical oxidation of arsenic(III) to
487 arsenic(V) using potassium peroxydisulfate as an oxidizing agent. Water Res. 44(12),
488 3687-3695.
489 Nesbitt, H.W., Canning, G.W. and Bancroft, G.M. 1998. XPS study of reductive dissolution of
490 7Å-birnessite by H_3AsO_3, with constraints on reaction mechanism. Geochim. Cosmochim. Acta
491 62(12), 2097-2110.
492 Nicholson, K. and Eley, M. 1997. Geochemistry of manganese oxides: metal adsorption in freshwater
493 and marine environments. Geological Society London Special Publications 119(1), 309-326.
494 Nico, P.S. and Zasoski, R.J. 2001. Mn(III) center availability as a rate controlling factor in the oxidation
495 of phenol and sulfide on δ-MnO_2. Environ. Sci. Technol. 35, 3338-3343.
496 Orriss, I.R., Arnett, T.R. and Russell, R.G. 2016. Pyrophosphate: a key inhibitor of mineralisation. Curr
497 Opin Pharmacol 28, 57-68.
498 Oscarson, D.W., Huang, P.M., Defosse, C. and Herbillon, A. 1981a. Oxidative power of Mn(IV) and
499 Fe(III) oxides with respect As(III) in terrestrial and aquatic envrionments. Nature 291, 50-51.
500 Oscarson, D.W., Huang, P.M. and Liaw, W.K. 1980. The oxidation of arsenite by aquatic sediments. J.
501 Environ. Qual. 9, 700-703.
502 Oscarson, D.W., Huang, P.M. and Liaw, W.K. 1981b. Role of manganese in the oxidation of arsenite by
503 freshwater lake sediments. Clay. Clay Miner. 29(3), 219-225.
504 Parikh, S.J., Lafferty, B.J., Meade, T.G. and Sparks, D.L. 2010. Evaluating environmental influences on
505 As^{III} oxidation kinetics by a poorly crystalline Mn-oxide. Environ. Sci. Technol. 44, 3772–3778.
506 Parker, D.L., Sposito, G. and Tebo, B.M. 2004. Manganese (III) binding to a pyoverdine siderophore

produced by a manganese (II)-oxidizing bacterium. Geochim. Cosmochim. Acta 68(23), 4809-4820.

Qian, A., Zhang, W., Shi, C., Pan, C., Giammar, D.E., Yuan, S., Zhang, H. and Wang, Z. 2019. Geochemical stability of dissolved Mn(III) in the presence of pyrophosphate as a model ligand: complexation and disproportionation. Environ. Sci. Technol. 53(10), 5768-5777.

Scott, M.J. and Morgan, J.J. 1995. Reactions at oxide surfaces. 1. Oxidation of As(lll) by synthetic birnessite. Environ. Sci. Technol. 29(8), 1898-1905.

Soldatova, A.V., Romano, C.A., Tao, L., Stich, T.A., Casey, W.H., Britt, R.D., Tebo, B.M. and Spiro, T.G. 2017. Mn(II) oxidation by the multicopper oxidase complex Mnx: A coordinated two-stage Mn(II)/(III) and Mn(III)/(IV) mechanism. J. Am. Chem. Soc. 139(33), 11381-11391.

Taube, H. 1947. Catalysis of the reaction of chlorine and oxalic acid. Complexes of trivalent manganese in solutions containing oxalic acid. J. Am. Chem. Soc. 69(6), 1418-1428.

Tournassat, C., Chalet, L., Bosbach, D. and Manceau, A. 2002. Arsenic(III) oxidation by birnessite and precipitation of manganese(II) arsenate. Environ. Sci. Technol. (36), 493-500.

Trouwborst, R.E., Clement, B.G., Tebo, B.M., Glazer, B.T. and Luther, G.W., 3rd 2006. Soluble Mn(III) in suboxic zones. Science 313(5795), 1955-1957.

Tsang, S., Phu, F., Baum, M.M. and Poskrebyshev, G.A. 2007. Determination of phosphate/arsenate by a modified molybdenum blue method and reduction of arsenate by S(2)O(4)(2-). Talanta 71(4), 1560-1568.

Villalobos, M., Escobar-Quiroz, I.N. and Salazar-Camacho, C. 2014. The influence of particle size and structure on the sorption and oxidation behavior of birnessite: I. Adsorption of As(V) and oxidation of As(III). Geochim. Cosmochim. Acta 125, 564-581.

Wan, B., Huang, R., Diaz, J.M. and Tang, Y. 2019. Manganese Oxide Catalyzed Hydrolysis of Polyphosphates. ACS Earth Space Chem. 3(11), 2623-2634.

Wang, L. and Giammar, D.E. 2015. Effects of pH, dissolved oxygen, and aqueous ferrous iron on the adsorption of arsenic to lepidocrocite. J. Colloid Interface Sci. 448, 331-338.

Wang, Q., Yang, P. and Zhu, M. 2018. Structural transformation of birnessite by fulvic acid under anoxic conditions. Environ. Sci. Technol. 52(4), 1844-1853.

Wang, Y. and Stone, A.T. 2006. Reaction of $Mn^{III,IV}$ (hydr)oxides with oxalic acid, glyoxylic acid, phosphonoformic acid, and structurally-related organic compounds. Geochim. Cosmochim. Acta 70(17), 4477-4490.

Wang, Z., Lv, K., Wang, G., Deng, K. and Tang, D. 2010. Study on the shape control and photocatalytic activity of high-energy anatase titania. Appl. Catal. B 100(1-2), 378-385.

Webb, S.M., Dick, G.J., Bargar, J.R. and Tebo, B.M. 2005. Evidence for the presence of Mn(III) intermediates in the bacterial oxidation of Mn(II). Proc. Natl. Acad. Sci. U S A 102(15), 5558-5563.

Wu, Y., Kukkadapu, R.K., Livi, K.J.T., Xu, W., Li, W. and Sparks, D.L. 2018. Iron and arsenic speciation during As(III) oxidation by manganese oxides in the presence of Fe(II): Molecular-level characterization using XAFS, Mössbauer, and TEM analysis. ACS Earth Space Chem. 2(3), 256-268.

Yang, T., Wen, W., Yin, G. and Gao, X. 2015. Introduction of the X-ray diffraction beamline. Nucl. Sci. Tech. 26(2), 020101.

Yang, X., Xia, L., Li, J., Dai, M., Yang, G. and Song, S. 2017. Adsorption of As (III) on porous hematite synthesized from goethite concentrate. Chemosphere 169, 188-193.

Yin, H., Kwon, K.D., Lee, J.-Y., Shen, Y., Zhao, H., Wang, X., Liu, F., Zhang, J. and Feng, X. 2017. Distinct effects of Al^{3+} doping on the structure and properties of hexagonal turbostratic birnessite: A comparison with Fe3+ doping. Geochim. Cosmochim. Acta 208, 268-284.

Ying, S.C., Kocar, B.D. and Fendorf, S. 2012. Oxidation and competitive retention of arsenic between iron- and manganese oxides. Geochim. Cosmochim. Acta 96, 294–303.

Zhang, C., Liao, X., Lü, Y. and Nan, C. 2019. Enhanced degradation of methyl parathion in the ligand stabilized soluble Mn(III)-sulfite system. J. Earth Sci. 30, 861–869.

Zhang, G., Qu, J., Liu, H., Liu, R. and Guo, T. 2007. Removal mechanism of As(III) by a novel Fe-Mn binary oxide adsorbent: Oxidation and sorption. Environ. Sci. Technol. 41, 4613-4619.

Zhang, L., Zhu, T., Liu, X. and Zhang, W. 2016. Simultaneous oxidation and adsorption of As (III) from water by cerium modified chitosan ultrafine nanobiosorbent. J. Hazard. Mater. 308, 1-10.

Zhang, W., Zhang, G., Liu, C., Li, J., Zheng, T., Ma, J., Wang, L., Jiang, J. and Zhai, X. 2018. Enhanced removal of arsenite and arsenate by a multifunctional Fe-Ti-Mn composite oxide: photooxidation, oxidation and adsorption. Water Res. 147, 264-275.

Zhao, W., Liu, F., Feng, X., Tan, W., Qiu, G. and Chen, X. 2012. Fourier transform infrared spectroscopy study of acid birnessites before and after Pb^{2+} adsorption. Clay Miner. 47(02), 191-204.

Zhao, Z., Jia, Y., Xu, L. and Zhao, S. 2011. Adsorption and heterogeneous oxidation of As (III) on ferrihydrite. Water Res. 45(19), 6496-6504.

Zheng, Q., Hou, J., Hartley, W., Ren, L., Wang, M., Tu, S. and Tan, W. 2020. As(III) adsorption on Fe-Mn binary oxides: Are Fe and Mn oxides synergistic or antagonistic for arsenic removal? Chem. Eng. J. 389, 124470.

Zhu, M., Paul, K.W., Kubicki, J.D. and Sparks, D.L. 2009. Quantum chemical study of arsenic (III, V) adsorption on Mn-oxides, implications for arsenic(III) oxidation. Environ. Sci. Technol. 43, 6655–6661.

Zhu, Y., Liang, X., Zhao, H., Yin, H., Liu, M., Liu, F. and Feng, X. 2017. Rapid determination of the Mn average oxidation state of Mn oxides with a novel two-step colorimetric method. Anal. Methods 9(1), 103-109.

Legends of figures and tables

Fig. 1 (a) Evolution of As(III), As(V), and total As concentrations in solution during As(III) oxidation by birnessite in the absence/presence of 5 mM PP (1.0 mM initial As(III) concentration, initial pH 7.2, 24 h). (b) Kinetic analysis of As(III) removal using pseudo-first order model.

Fig. 2 (a) Evolution of aqueous Mn species concentrations in solution during As(III) oxidation by birnessite in the absence/presence of 5 mM PP (1.0 mM initial As(III)

586 concentration, initial pH 7.2, 24 h). (b) Evolution as a function of reaction time of
587 UV-Vis absorption spectra of the solutions containing Mn(III)-PP as the result of
588 As(III) oxidation experiments (dilution in 1:5 in deionized water) in the presence of
589 birnessite and PP (5 mM PP, 1.0 mM initial As(III) concentration, initial pH 7.2).
590 **Fig. 3** As(III), As(V), and Mn concentrations in solution and the ratio between Mn and
591 As(V) as a function of the pyrophosphate (PP) concentration for As(III) oxidation
592 experiments in the presence of birnessite (1.0 mM initial As(III) concentration, initial
593 pH 7.2, 24 h).
594 **Fig. 4** FESEM images of unreacted synthetic birnessite (Bir) and of reaction products
595 from As(III) oxidation experiments in the presence of birnessite (1.0 mM initial As(III)
596 concentration, initial pH 7.2, 24 h). 0mM: absence of pyrophosphate (PP); 2mM:
597 initial PP concentration 2 mM; 5mM: initial PP concentration 5 mM.
598 **Fig. 5** (a) XRD patterns and (b) FT-IR spectra of unreacted birnessite (Bir) and of
599 solid reaction products from As(III) oxidation experiments in the presence of
600 birnessite (1.0 mM initial As(III) concentration, initial pH 7.2, 24 h). 0mM, 2mM, and
601 5mM labels as in Fig. 4. Ticks at the bottom of (a) indicate the position of manganite
602 reflections (ICDD#41-1379).
603 **Fig. 6** XPS spectra (Mn*3p*) of unreacted birnessite (Bir) and of solid reaction products
604 from As(III) oxidation experiments in the presence of birnessite (1.0 mM initial As(III)
605 concentration, initial pH 7.2, 24 h). 0mM, 2mM, and 5mM labels as in Fig. 4.
606 **Fig. 7** Evolution of (a) As(III), As(V), and total As concentrations, and of (b) aqueous
607 Mn species concentrations during As(III) oxidation by birnessite in the

608 absence/presence of 5 mM oxalate (1.0 mM initial As(III) concentration, initial pH
609 7.2, 24 h).

610 **Table 1** Relative proportions of the different Mn oxidation states at the birnessite
611 surface determined from the fits of Mn*3p* XPS spectra shown in Fig. 6.

Tables

Table 1

Relative proportions of the different Mn oxidation states determined from the fits of Mn*3p* XPS spectra shown in Fig. 6.

Samples	Mn (At.%)			
	Mn(IV)	Mn(III)	Mn(II)	AOS
Bir	67	29	4	3.63
0 mM PP 1 mM As(III)	41	50	9	3.32
2 mM PP 1 mM As(III)	46	42	12	3.34
5 mM PP 1 mM As(III)	49	38	13	3.35

Figure

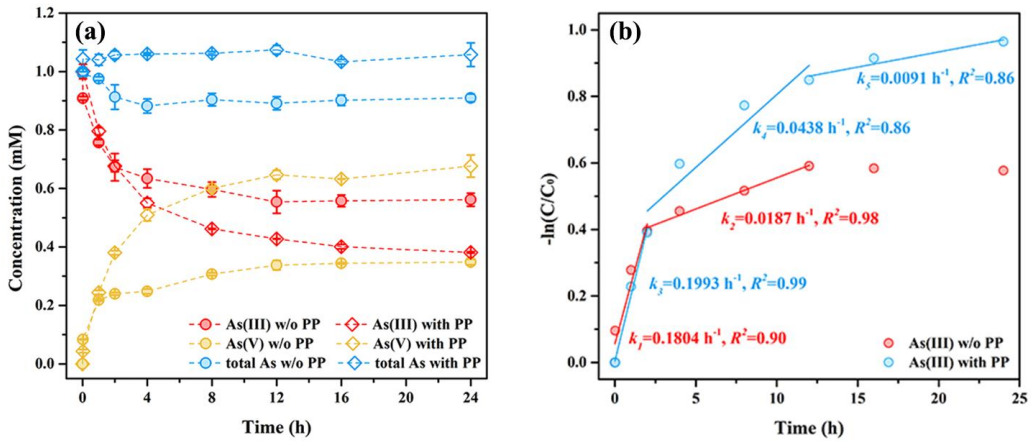

Fig. 1 (a) Evolution of As(III), As(V), and total As concentrations in solution during As(III) oxidation by birnessite in the absence/presence of 5 mM PP (1.0 mM initial As(III) concentration, initial pH 7.2, 24 h). (b) Kinetic analysis of As(III) removal using pseudo-first order model.

Figure

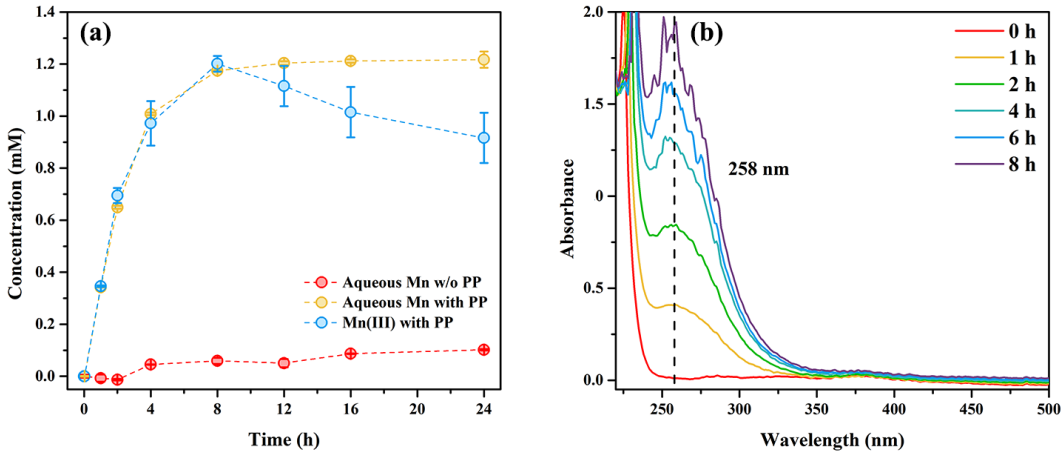

Fig. 2 (a) Evolution of aqueous Mn species concentrations in solution during As(III) oxidation by birnessite in the absence/presence of 5 mM PP (1.0 mM initial As(III) concentration, initial pH 7.2, 24 h). (b) Evolution as a function of reaction time of UV-Vis absorption spectra of the solutions containing Mn(III)-PP as the result of As(III) oxidation experiments (dilution in 1:5 in deionized water) in the presence of birnessite and PP (5 mM PP, 1.0 mM initial As(III) concentration, initial pH 7.2).

Figure

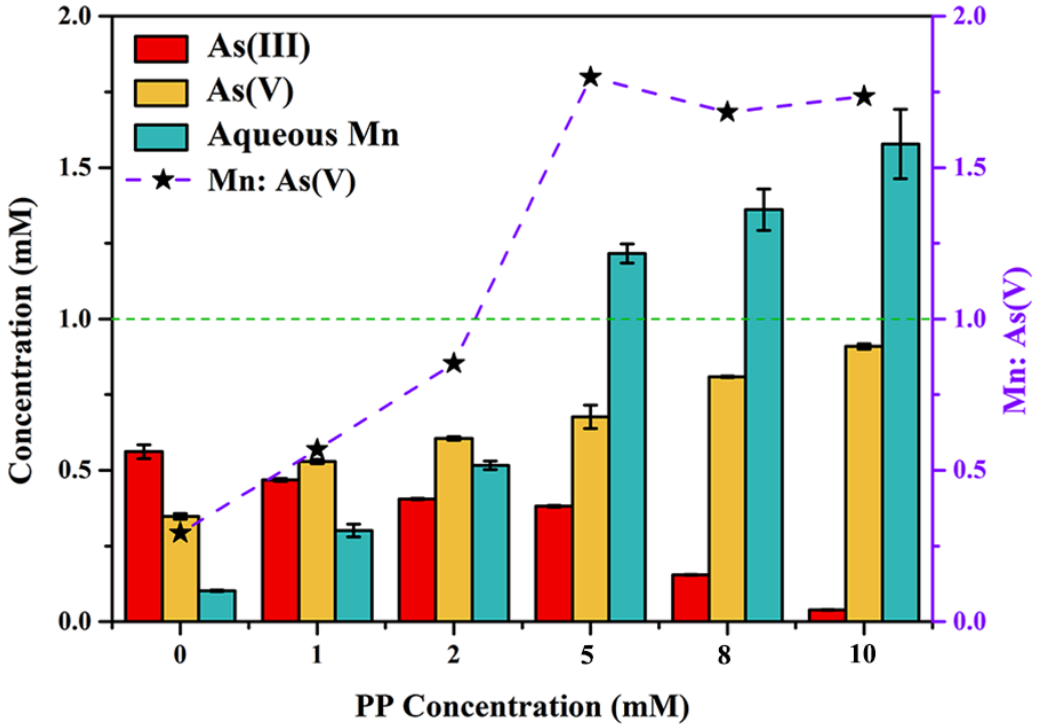

Fig. 3 As(III), As(V), and Mn concentrations in solution and the ratio between Mn and As(V) as a function of the pyrophosphate (PP) concentration for As(III) oxidation experiments in the presence of birnessite (1.0 mM initial As(III) concentration, initial pH 7.2, 24 h).

Figure

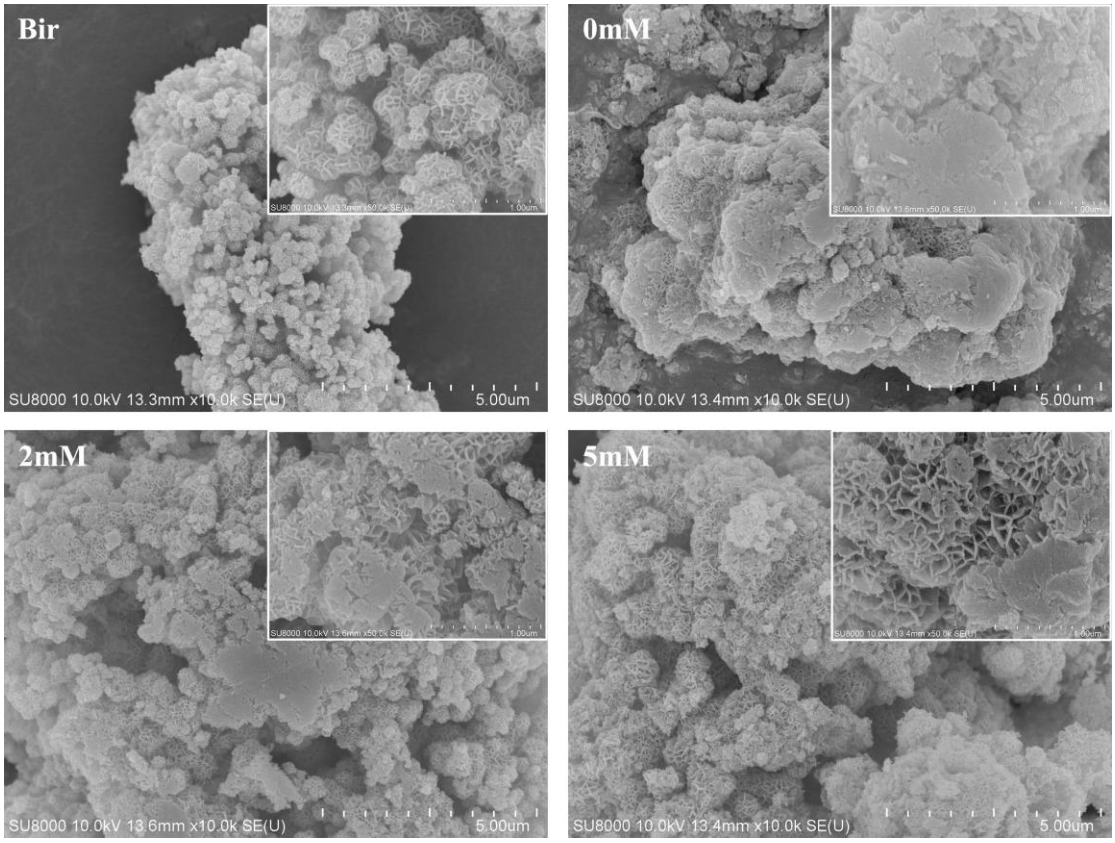

Fig. 4 FESEM images of unreacted synthetic birnessite (Bir) and of reaction products from As(III) oxidation experiments in the presence of birnessite (1.0 mM initial As(III) concentration, initial pH 7.2, 24 h). 0mM: absence of pyrophosphate (PP); 2mM: initial PP concentration 2 mM; 5mM: initial PP concentration 5 mM.

Figure

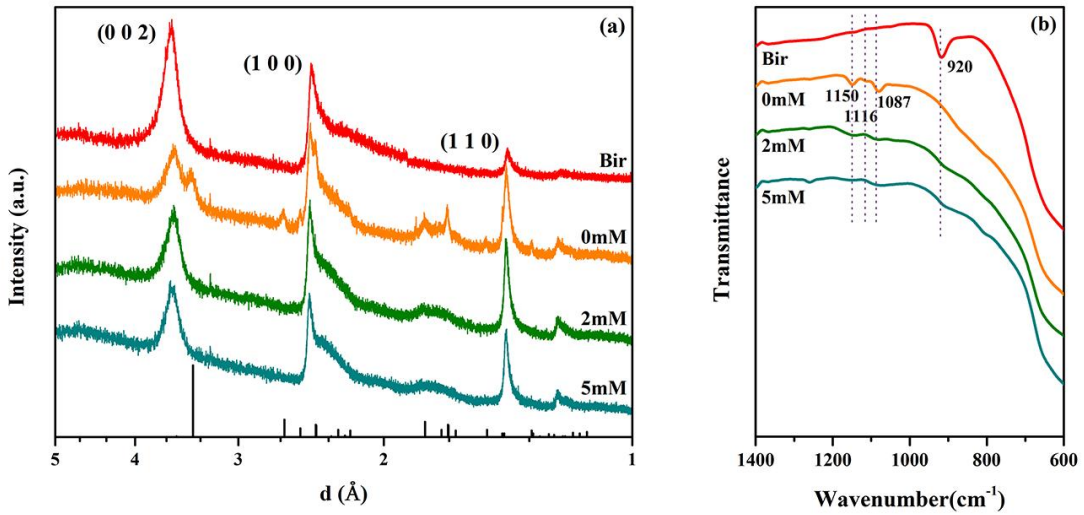

Fig. 5 (a) XRD patterns and (b) FT-IR spectra of unreacted birnessite (Bir) and of solid reaction products from As(III) oxidation experiments in the presence of birnessite (1.0 mM initial As(III) concentration, initial pH 7.2, 24 h). 0mM, 2mM, and 5mM labels as in Fig. 4. Ticks at the bottom of (a) indicate the position of manganite reflections (ICDD#41-1379).

Figure

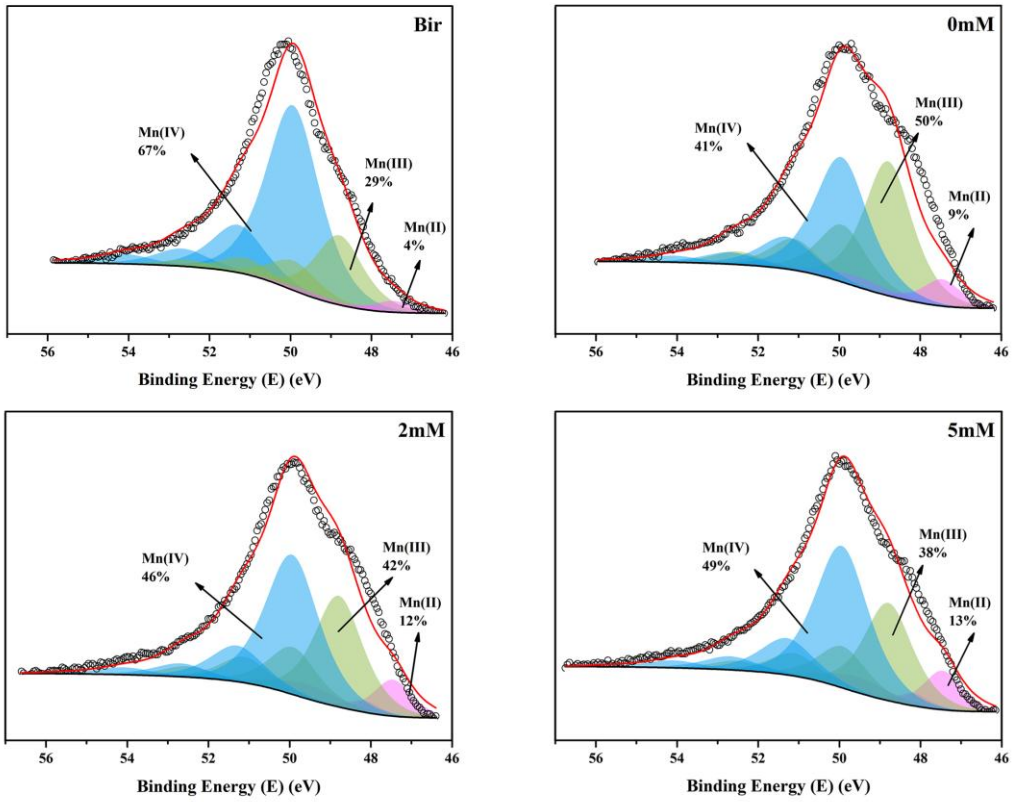

Fig. 6 XPS spectra (Mn3p) of unreacted birnessite (Bir) and of solid reaction products from As(III) oxidation experiments in the presence of birnessite (1.0 mM initial As(III) concentration, initial pH 7.2, 24 h). 0mM, 2mM, and 5mM labels as in Fig. 4.

Figure

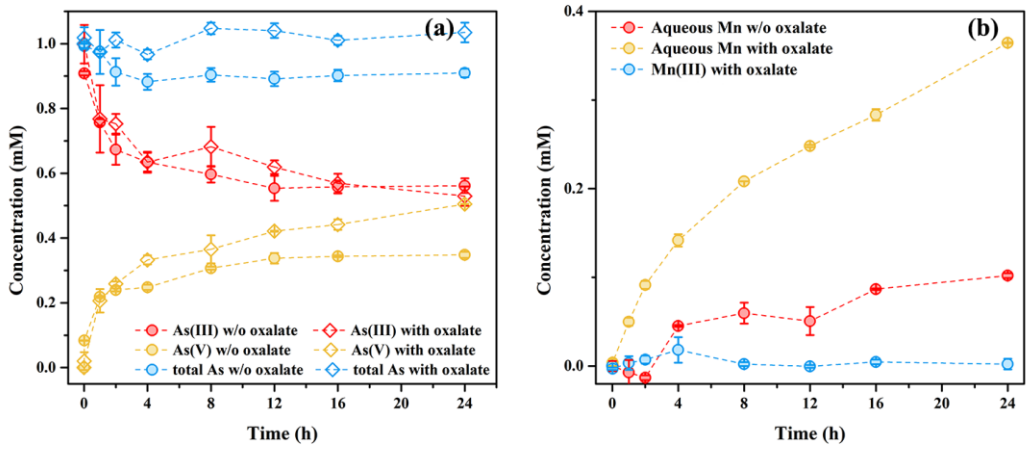

Fig. 7 Evolution of (a) As(III), As(V), and total As concentrations, and of (b) aqueous Mn species concentrations during As(III) oxidation by birnessite in the absence/presence of 5 mM oxalate (1.0 mM initial As(III) concentration, initial pH 7.2, 24 h).

Supporting information to

Highly enhanced oxidation of arsenite at the surface of birnessite in the presence of pyrophosphate and the underlying reaction mechanisms

Chaoyun Ying[a], Bruno Lanson[b], Cheng Wang[a], Xiaoming Wang[a], Hui Yin[a], Yupeng Yan[a], Wenfeng Tan[a], Fan Liu[a], Xionghan Feng[a,]*

[a]Key Laboratory of Arable Land Conservation (Middle and Lower Reaches of Yangtze River), Ministry of Agriculture, College of Resources and Environment, Huazhong Agricultural University, Wuhan 430070, China.

[b]Univ. Grenoble Alpes, CNRS, Univ. Savoie Mont Blanc, IRD, Univ. Gustave Eiffel, ISTerre, F-38000 Grenoble, France

This PDF file includes:

Materials and Methods

In-situ quick As K-edge XANES spectroscopy.

In-situ quick As K-edge X-ray Absorption Near Edge Structure (XANES) spectroscopy data were collected at ~25 ℃ at the 1W2B beamline of Beijing Synchrotron Radiation Facility in fluorescence mode, to track the evolution of As(III) and As(V) relative proportions during the oxidation of 2.0 mM As(III) in the presence of 1.6 g/L birnessite and 5 mM PP at pH ~7.5. Experimental conditions were similar to those reported by Ginder-Vogel et al. (2009) and could be described as follows. The 50 mL suspensions were stirred in 100 mL plastic beakers with a small hole (Ø = 1 cm) close to the bottom. The spectroscopy data were continuously collected as a function of reaction time between 11.67 and 12.46 keV. Elementary spectra were collected within 40 s each. The Athena program was used for background removal and linear combination fittings (LCF) for quantifying the speciation variations of As using As(III) and As(V) references.

Table S1

Evolution as a function of time of the solution UV-Vis absorbance at 480 nm from As(III) oxidation experiments in the presence of Mn(III)-PP (0.5 mM initial As(III) concentration, initial pH 7.2). Blank experiments without As(III) were also conducted.

Samples	0.5 mM Mn(III)-PP ($Abs_{480\ nm}$)		1 mM Mn(III)-PP ($Abs_{480\ nm}$)	
	0.5 mM As(III)	No As(III)	0.5 mM As(III)	No As(III)
0 h	0.0363	0.0368	0.0720	0.0684
24 h	0.0355	0.0372	0.0726	0.0690

Table S2

Parameters used for fitting Mn*3p* XPS spectra of birnessite before and after As(III) oxidation in the absence/presence of PP (from Ilton et al., 2016).

	Binding Energy (eV)	FWHM (eV)
Mn(II)*3p* Parameters		
Mn(II)	47.46	1.12
Mn(II)	48.16	0.93
Mn(II)	49.59	1.97
Mn(III)*3p* Parameters		
Mn(III)	48.79	1.42
Mn(III)	49.92	1.42
Mn(III)	51.11	1.42
Mn(III)	52.52	1.42
Mn(III)	46.57	1.21
Mn(IV)*3p* Parameters		
Mn(IV)	49.94	1.57
Mn(IV)	51.29	1.57
Mn(IV)	52.68	1.57
Mn(IV)	54.08	1.57
Mn(IV)	55.56	1.71

Table S3

Parameters used for fitting As*3d* XPS spectra of birnessite before and after As(III) oxidation in the absence/presence of PP (from Bang et al., 2005).

	Binding Energy (eV)	FWHM (eV)
As*3d* Parameters		
As(III)	44.20	1.39
As(V)	45.40	1.32

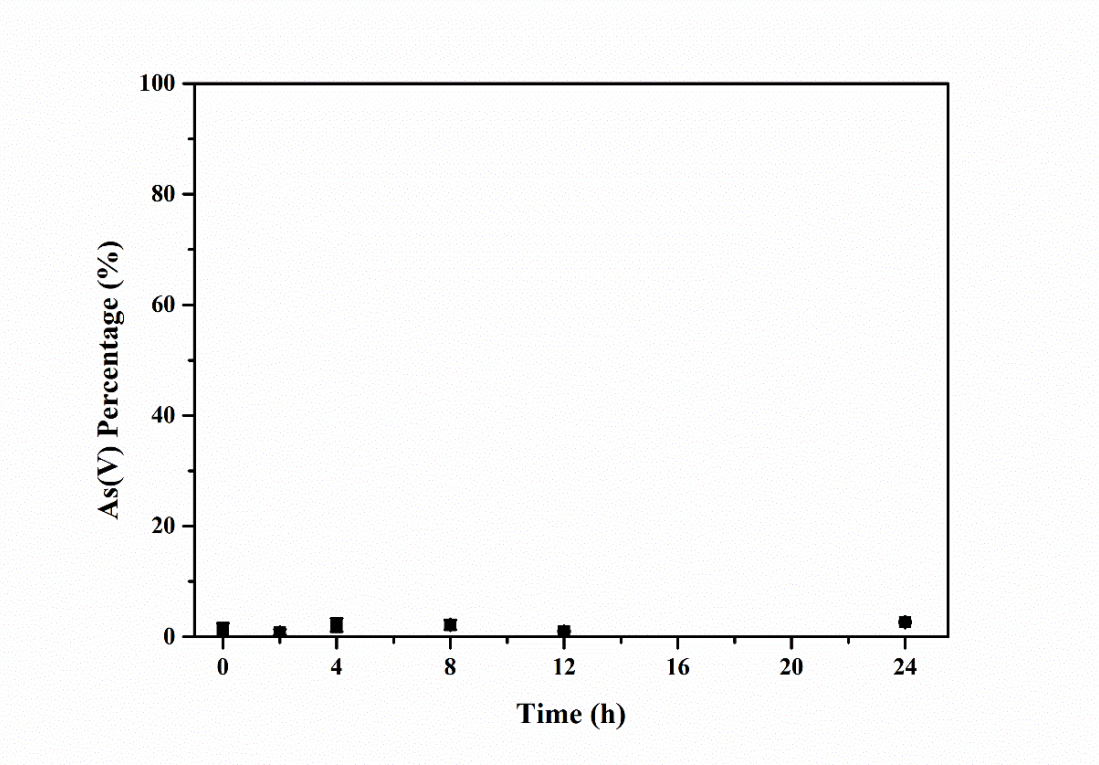

Fig. S1 Evolution of As(V) relative proportion during an As(III) oxidation experiment in the absence of birnessite (0.5 mM initial As(III) concentration, initial pH 7.2).

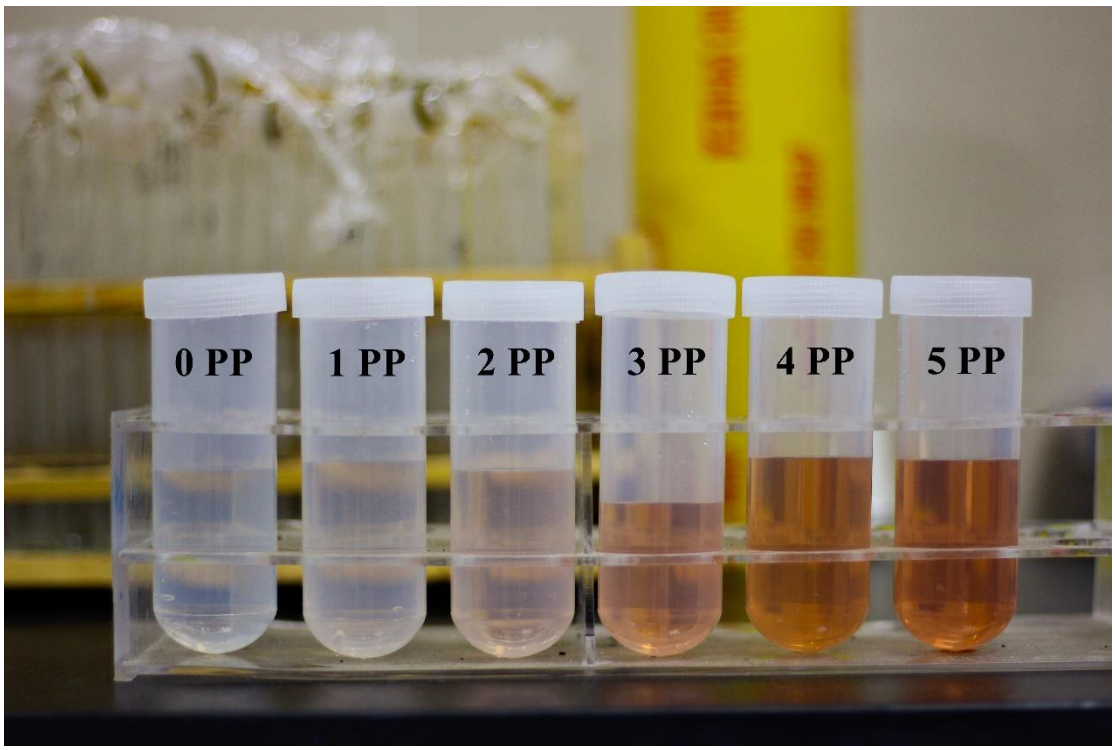

Fig. S2 Evolution of solution color from As(III) oxidation experiments performed in the presence of birnessite with variable initial concentrations of PP (0.5 mM initial As(III) concentration, initial pH 7.2, 24 h).

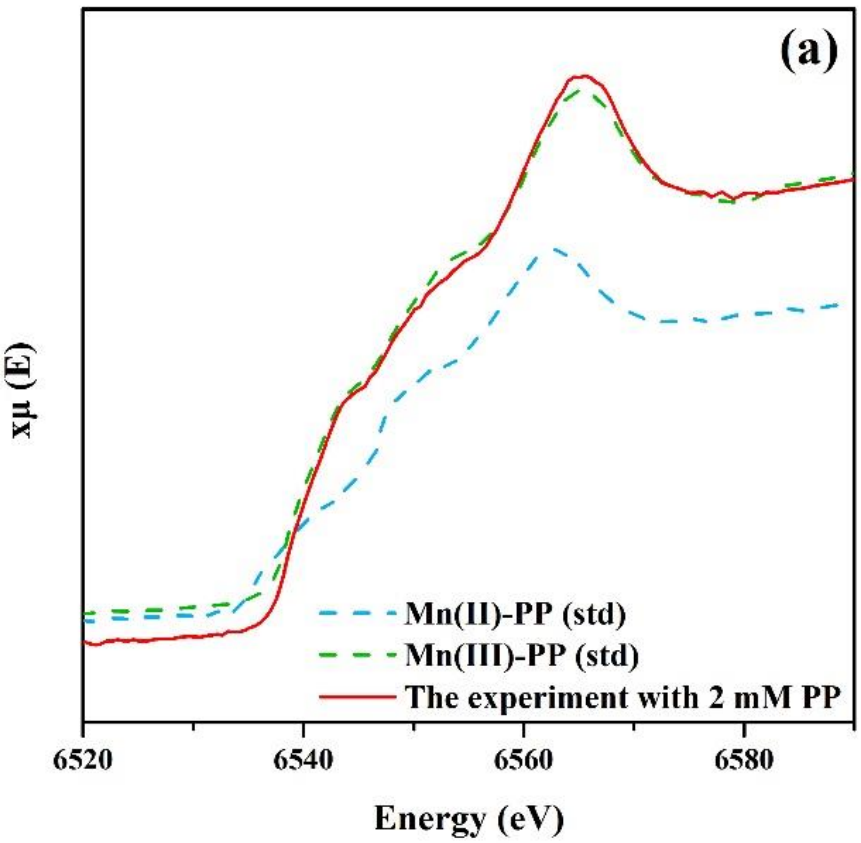

Fig. S3 Mn K-edge XANES spectrum of the solution resulting from an As(III) oxidation experiment in the presence of birnessite (1.0 mM initial As(III) concentration, 2mM initial PP concentration, initial pH 7.2, 24 h) compared with Mn(II)-PP and Mn(III)-PP reference spectra.

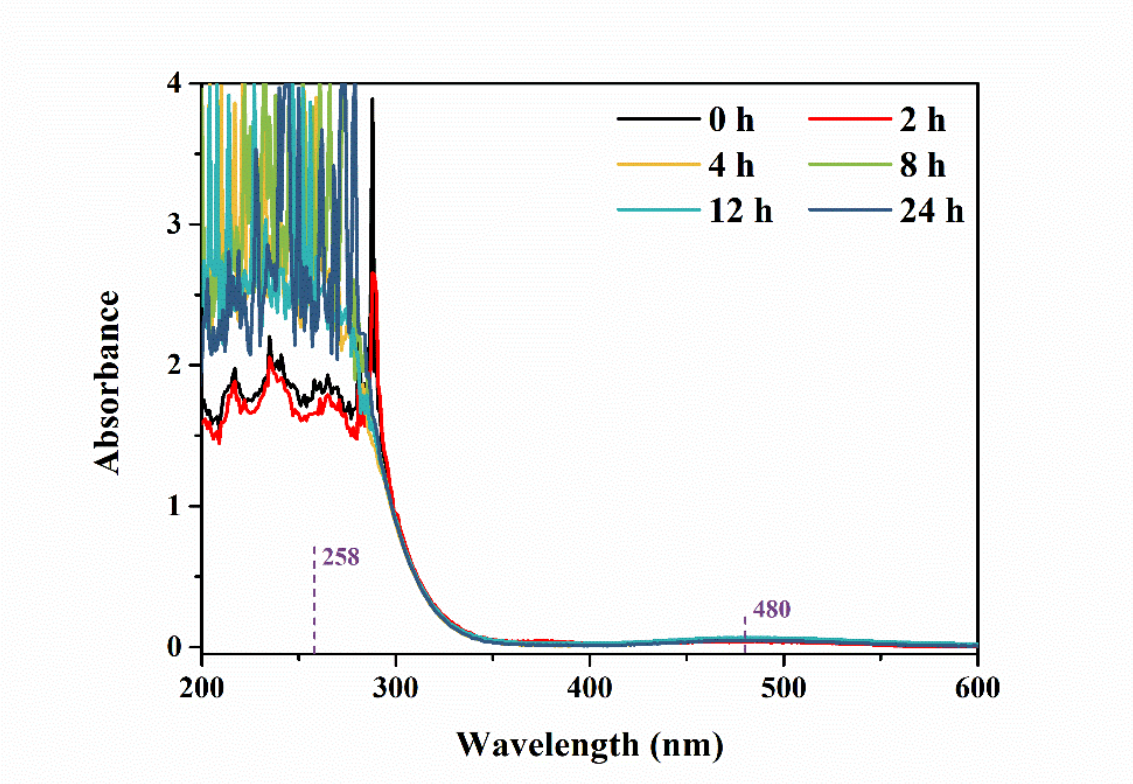

106

107 **Fig. S4** Evolution as a function of time of UV-Vis absorption spectra of a solution

108 containing 0.5 mM Mn(III)-PP and 0.5 mM As(V) (initial pH 7.2, 24 h).

109

110

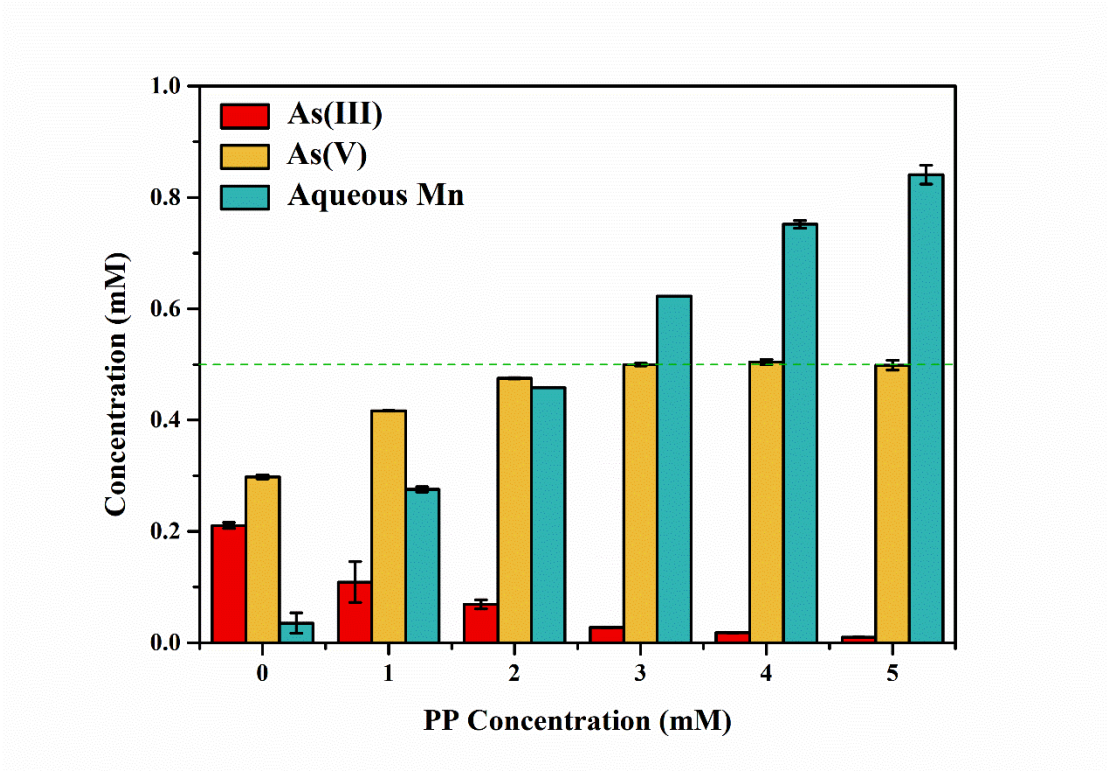

Fig. S5 As(III), As(V), and Mn concentrations in solution as a function of the pyrophosphate (PP) concentration for As(III) oxidation experiments in the presence of birnessite (0.5 mM initial As(III) concentration, initial pH 7.2, 24 h).

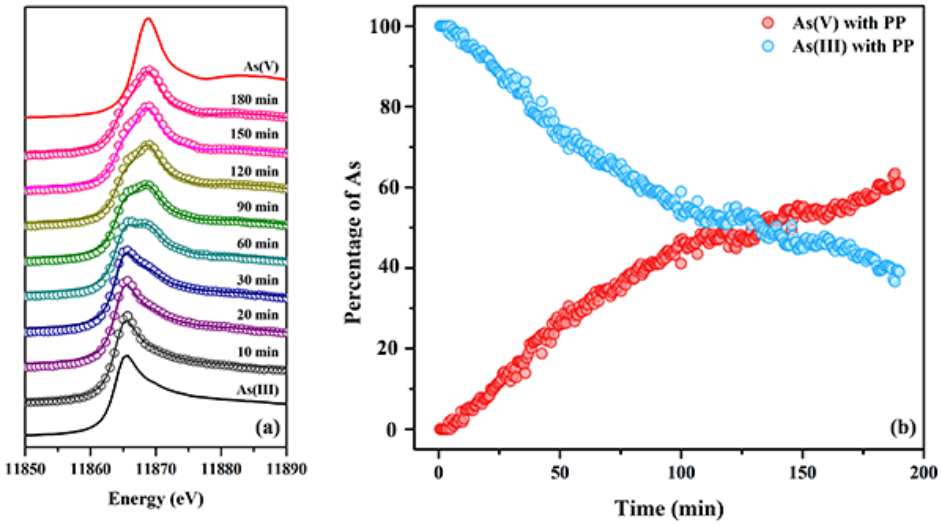

118

119 **Fig. S6** (a) Selected As K-edge XAS spectra used to determine the relative proportions

120 of As(III) and As(V) during an As(III) oxidation experiment in the presence of

121 birnessite (2.0 mM initial As(III) concentration, 1.6 g/L initial birnessite, 5 mM PP

122 concentration, initial pH 7.5), (b) Evolution as a function of time of the relative

123 proportions of As(III) and As(V) determined from the linear combination fitting (LCF)

124 of the As K-edge XAS data shown in (a).

125

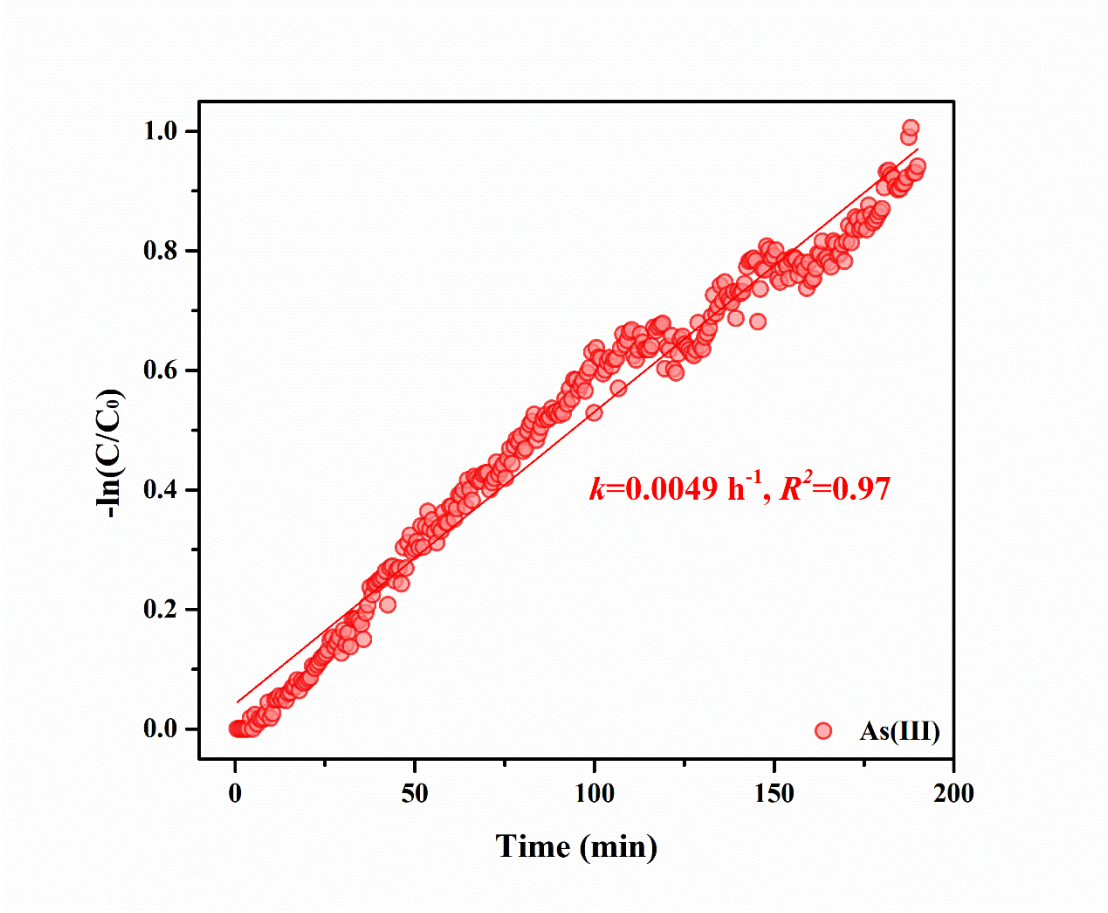

126

127 **Fig. S7** Kinetic analysis of As(III) removal deduced from the linear combination fitting

128 (LCF) results of As K-edge XANES spectra shown in Fig. S6(b) using pseudo-first

129 order model (2.0 mM initial As(III) concentration, 1.6 g/L initial birnessite, 5 mM PP

130 concentration, initial pH 7.5).

131

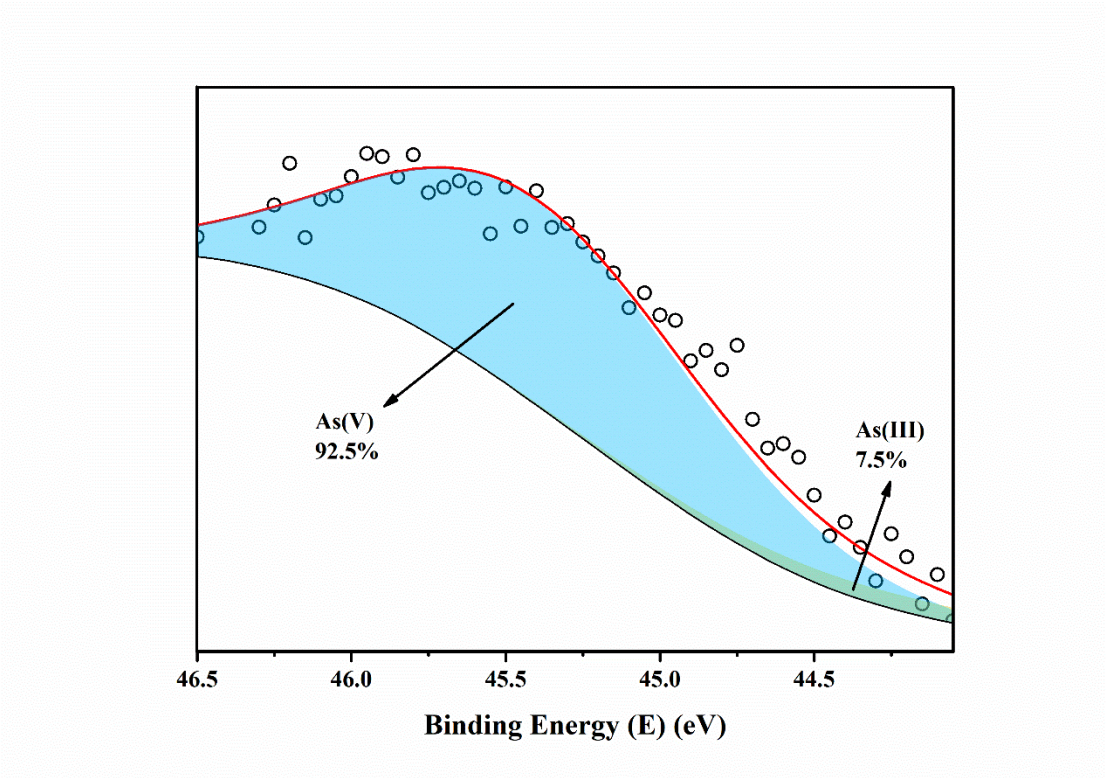

Fig. S8 As*3d* XPS spectrum of reaction products from an As(III) oxidation experiment in the presence of birnessite and absence of PP (1.0 mM initial As(III) concentration, initial pH 7.2, 24 h).

References

Bang, S., Johnson, M.D., Korfiatis, G.P. and Meng, X. 2005. Chemical reactions between arsenic and zero-valent iron in water. Water Res. 39(5), 763-770.

Ginder-Vogel, M., Landrot, G., Fischel, J.S. and Sparks, D.L. 2009. Quantification of rapid environmental redox processes with quick-scanning X-ray absorption spectroscopy (Q-XAS). Proc. Natl. Acad. Sci. U S A 106(38), 16124-16128.

Ilton, E.S., Post, J.E., Heaney, P.J., Ling, F.T. and Kerisit, S.N. 2016. XPS determination of Mn oxidation states in Mn (hydr)oxides. Appl. Surf. Sci. 366, 475-485.